

# Particle-Size-Grouping Model of Precipitation Kinetics in Microalloyed Steels

Kun Xu, Brian G. Thomas

Mechanical Science and Engineering Department

University of Illinois at Urbana-Champaign

1206 West Green St., Urbana, IL 61801, USA

Phone – (217) 333-6919

Fax – (217) 244-6534

Email: [kunxu2@illinois.edu](mailto:kunxu2@illinois.edu), [bgthomas@illinois.edu](mailto:bgthomas@illinois.edu)

**Abstract:** The formation, growth, and size distribution of precipitates greatly affects the microstructure and properties of microalloyed steels. The computational Particle-Size-Grouping (PSG) kinetic models were developed to simulate precipitate particle growth due to collision and diffusion mechanisms. Firstly, the standard PSG method for collision is clearly explained and verified. Then a new PSG method is proposed for the diffusion-controlled precipitate growth with complete mass conservation. In comparison with the original population calculation, the PSG method saves significant computation and preserves enough accuracy for system with a large range of particle sizes. Finally the new PSG method is applied to simulate the precipitated fraction of AlN, and size distribution of NbC during isothermal ageing processing, and good matches are found with experimental measurements.

## 1. Introduction

The demand for steels with higher strength, ductility, and toughness is always increasing. Many alloying additions act to improve these properties through the formation of precipitate particles. In addition to the precipitation strengthening, the precipitates often act by pinning grain boundaries and inhibiting grain growth during steel processes. This effect arises from the disappearance of a small area of grain boundary when it intersects a second phase particle, and is widely acknowledged to depend on the volume fraction and particle size of the precipitates<sup>[1-4]</sup>. Many small particles are more effective than a few large particles. An unfortunate side effect is a decrease in high temperature ductility and possible crack formation during processes such as casting and hot rolling due to the growth of voids around precipitate particles on the weak grain boundaries. It is therefore important to control the spatial distribution, morphological characteristics, and size distribution of precipitates during all stages of steel processing. These parameters are generally determined by the alloy composition, and temperature history. In high-deformation processes such as rolling, they also strongly depend upon strain and strain rate.

The accurate modeling of precipitate growth has at least two analysis steps: 1) supersaturation, based on equilibrium precipitation thermodynamics, 2) kinetic effects. Many models to predict equilibrium precipitation are available in commercial packages based on minimizing Gibbs free energy, including Thermo calc<sup>[5,6]</sup>, FactSage<sup>[7]</sup>, ChemSage<sup>[8]</sup>, JMatPro<sup>[9]</sup>, other CALPHAD models<sup>[10,11]</sup>, and other thermodynamic models based on solubility products in previous literature<sup>[12-16]</sup>. A recent equilibrium model efficiently predicts the stable formation of typical oxides, sulfides, nitrides and carbides in microalloyed steels, by solving the fully-coupled nonlinear system of solubility-product equations<sup>[17]</sup>. Mutual solubility is incorporated for appropriate precipitates with similar crystal structures and lattice parameters. This model includes the solubility limit of precipitates in different steel phases, influence of Wagner interaction on activities and complete mass conservation of alloying elements during precipitation. The model has been widely validated with analytical solutions of simple cases, results of a commercial package, and previous experimental results<sup>[17]</sup>. A useful equilibrium model must accurately predict the occurrence and stability of precipitates, their equilibrium amounts, and compositions, for different steel compositions, phases, and temperatures, in order to calculate the supersaturation/driving force for a kinetic model.

Theoretically, precipitates start to form when the solubility limit is exceeded, but reaching equilibrium usually takes a long time. For most steel processes, especially at lower temperatures, equilibrium is seldom approached due to limited time. Thus, kinetic models of precipitate growth are a practical necessity for realistic predictions.

An early effort to predict phase transformation kinetics is the KJMA model, by Kolmogorov<sup>[18]</sup>, Johnson, Mehl<sup>[19]</sup> and Avrami<sup>[20]</sup>, which is widely used to study precipitation processes and to generate TTT diagrams. The general isothermal KJMA equation to describe transformed fraction,  $f$ , as a function of time,  $t$ , is given by<sup>[21]</sup>

$$f(t) = 1 - \exp(-K \cdot t^n) \quad [1]$$

where  $K$  is the rate function for nucleation and growth which depends on chemical composition and temperature, and  $n$  is the Avrami exponent typically ranging from 1-4, which depends on growth dimensionality (1-D, 2-D or 3-D), nucleation index (zero, decreasing, constant or increasing nucleation rate), and growth index (interface-controlled or diffusion-controlled). The parameters  $K$  and  $n$  are determined from experimental measurements at different test temperatures and compositions, and often vary during precipitation. Although this model was successfully applied to match some precipitated fraction measurements<sup>[22,23]</sup>, its empirical nature prevents it from describing alternate thermomechanical processes without refitting the empirical parameters with further measurements. Moreover, size distributions are not predicted with this model.

Precipitates can form at different stages and locations in steelmaking, including: in the liquid steel due to collision, the mushy-zone between dendrites due to rapid diffusion during solidification, and on

the grain boundaries or inside the grains due to slow solid-state diffusion. This results in different composition, morphology and size distribution of precipitates, thus greatly influences the steel product qualities. Precipitate particles grow via two major mechanisms: 1) collision in liquid steel, 2) diffusion in both liquid and solid steel. Both mechanisms have been studied extensively, and better computational models are now available with fast improved computer power in recent decades.

Collisions between particles and rapid diffusion in the liquid phase increases the number of large particles, and enhances inclusion removal by flotation. The evolution of particle concentration and size distribution due to collisions has been described by the collision frequency between particles per unit volume of liquid medium<sup>[24]</sup>, and such models have been successfully applied for various collision mechanisms, including turbulent collision<sup>[25]</sup>, Stokes collision<sup>[26]</sup>, Brownian collision<sup>[27]</sup> and gradient collision<sup>[28]</sup>.

The entire diffusion-controlled precipitation process in solid typically includes nucleation, growth and coarsening stages. The nucleation stage includes an induction period to form stable nuclei, followed by steady-state nucleation, where the number of new particles increases linearly with time<sup>[29]</sup>. Such a classical nucleation model<sup>[29]</sup> has been successfully applied to predict the start of strain-induced Ti(C,N) precipitation in austenite<sup>[30]</sup>, and the results agree well with measurements inferred from stress relaxation experiments<sup>[31]</sup>.

After nucleation, particles of all sizes can grow due to the high supersaturation that defines the growth stage. After the nucleation and growth stages, precipitates of various sizes are dispersed in the matrix phase. Once the supersaturation has decreased to equilibrium ( $\sim 1$ ), the solute concentrations in the matrix and at the particle/matrix interface are comparable and capillary effects become dominant, causing coarsening or Ostwald ripening<sup>[32]</sup>. Governed by the minimization of the total surface energy, coarsening is driven by the difference in concentration gradients near precipitate particles of different sizes. The larger particles are surrounded by low concentration, so grow by diffusion from the high concentration surrounding smaller particles, which are less stable and shrink. Thus, the net number density of all particles now decreases with time.

Each of these three stages is dominated by different mechanisms, and particle size evolution follows different laws. Coarsening increases with time according to the mean particle size cubed<sup>[33,34]</sup>, which is slower than the square relation during the growth stage<sup>[35]</sup>. More discussion is given elsewhere on nucleation<sup>[36]</sup>, growth<sup>[37]</sup> and coarsening<sup>[38]</sup> phenomena.

Although the above phenomena describing precipitation kinetics are well established, most models of nucleation, growth and coarsening are empirical curve-fits, with separate calibration parameters for each stage. Moreover, they required simplified conditions and calculate only the variation of mean precipitate size with time. Little information on the size distribution can be obtained. But, different precipitate size distributions can have very different pinning effects on grain growth, even with the same mean size. Thus a fundamental model including all possible precipitation mechanisms is needed.

Molecule-based models such as Smoluchowski<sup>[24]</sup> for collision and Kampmann<sup>[39]</sup> for diffusion are attractive because the particles agglomerate automatically and the few parameters are fundamental physical constants themselves. Unfortunately, they encounter inevitable difficulties when they are applied to simulate practical processes, where precipitate size ranges greatly from nuclei  $\sim 0.1\text{nm}$  to coarsened particles larger than  $100\mu\text{m}$ . Realistic particles range in size over at least 6 orders of magnitude, and contain from 1 to  $10^{18}$  single molecules. With such an overwhelming linear scale, it is impossible to solve realistic problems using traditional models based on molecules.

Attempting to overcome this difficulty, the particle-size-group (PSG) method has been introduced in several previous studies<sup>[45],9</sup> and has proven to be very effective in calculating the evolution of particle size distributions for collision-coagulation growth over a large size range. Rather than track each individual particle size, the main idea of this technique is to divide the entire particle size range into a set of size classes, each with a specific mean size and size range. Careful attention is required to formulate the equations to ensure mass conservation<sup>[45]</sup>. Several researchers have applied this PSG method to simulate inclusion agglomeration in liquid steel due to collisions, coagulation and removal. Such models have been applied to RH degassers<sup>[40]</sup>, continuous casting tundishes<sup>[41,42]</sup> and ladle refining<sup>[43,44]</sup>. To start these PSG models, an initial size distribution is still required, which can be found from either experimental measurements or assumptions.

To make the PSG method more usable, Nakaoka *et al.*<sup>[46]</sup> used different volume ratios between neighboring size groups, taking advantage of the exponential increase in sizes that accompany powers of 2. This innovation allows modeling from single molecules to realistic particle sizes with only 30-50 size groups. Particle collisions were modeled, considering both inter-group and intra-group interactions, and numerical results agreed well with experimental agglomeration curves. However, very little work has been done to apply the PSG method to diffusion, which is the dominant mechanism for precipitate growth in many processes including steel casting and rolling. One study by Zhang and Pluschke<sup>[47]</sup>, coupled both collision and diffusion into a PSG model, but intra-group diffusion was not considered. Zhang<sup>[48]</sup> included a discrete-sectional technique by Gelbard<sup>[49]</sup> and Wu<sup>[50]</sup> into the PSG model, but this weakens the efficiency of the method and the accuracy of the treatment of diffusion and the insurance of mass conservation has not been verified. No previous study has demonstrated accurate simulation of diffusion using a PSG model.

The purpose of the present study is to develop accurate PSG methods to simulate precipitate growth due to both collision and diffusion mechanisms. The standard PSG method for collision problem is developed first, and a new PSG method is created. Both methods are verified by comparison with exact solutions of the primary population equations in test problems. The new PSG method is shown to be a very time-efficient calculation with complete mass balance and high accuracy. Finally, the new PSG method is applied to simulate several practical precipitation processes in solid steels, and compared with experimental measurements.

## 2. Models of precipitate growth mechanisms

### 2.1 Particle collision

The population balance model for collision first suggested by Smoluchowski<sup>[24]</sup> is:

$$\frac{dn_i}{dt} = \frac{1}{2} \sum_{k=1}^{i-1} \Phi_{k,i-k} n_k n_{i-k} - n_i \sum_{k=1}^{\infty} \Phi_{i,k} n_k \quad [2]$$

where  $n_i$  is the number of size  $i$  particles per unit volume, or “number density”, and  $\Phi_{i,j}$  is the collision kernel between size  $i$  and size  $j$  particles. The first term on the right-hand side generates size  $i$  particles due to the collision of two smaller particles, and the second term decreases the number of size  $i$  particles by their collision with particles of any size to become larger particles. The generation term is halved to avoid counting collision pairs twice. However, when two particles generating size  $i$  particles have same size, the generation term should not be halved because the collision pair is unique. Moreover, the loss term should be doubly counted when size  $i$  particles collide with themselves. The number of molecules composing the largest agglomerated particle must be a finite number  $i_M$  in numerical computation. Making these appropriate changes gives the following improved expression:

$$\frac{dn_i}{dt} = \frac{1}{2} \sum_{k=1}^{i-1} (1 + \delta_{k,i-k}) \Phi_{k,i-k} n_k n_{i-k} - n_i \sum_{k=1}^{i_M} (1 + \delta_{i,k}) \Phi_{i,k} n_k \quad [3]$$

where  $\delta_{i,k}$  is the Kronecker delta,  $\delta_{i,k}=1$  for  $i=k$  and  $\delta_{i,k}=0$  for  $i \neq k$ .

When  $i=1$ , the population balance for dissolved single molecules simplifies to:

$$\frac{dn_1}{dt} = -n_1 \sum_{k=1}^{i_M} (1 + \delta_{1,k}) \Phi_{1,k} n_k \quad [4]$$

Thus the number density of single molecules always decreases with collisions. Evaluating equations [3]-[4] requires summing over and tracking every possible size from 1 to  $i_M$  molecules, so is not practical for realistic particle sizes. Results from these equations, however, comprise the exact solution for collision test problems.

### 2.2 Particle diffusion

Kampmann<sup>[39]</sup> suggested the following diffusion-controlled model to treat the kinetics of nucleation, growth and coarsening as one continuous and simultaneous process.

$$\frac{dn_i}{dt} = -\beta_i n_1 n_i + \beta_{i-1} n_1 n_{i-1} - \alpha_i A_i n_i + \alpha_{i+1} A_{i+1} n_{i+1} \quad (i \geq 2) \quad [5]$$

where  $\beta_i$ ,  $\alpha_i$  and  $A_i$  are the diffusion growth rate, dissociation rate and reaction sphere surface area for a size  $i$  particle containing  $i$  molecules. The first and second terms on the right-hand side account for the loss and generation of size  $i$  particles due to “diffusion growth” by adding single molecules to

particle. The third and fourth terms account for the loss and generation of size  $i$  particles due to particle “dissociation” from losing single molecules. The effects of equilibrium, diffusion growth, curvature effects and mass balance are all included, with all the parameters having appropriate physical significance.

For single molecules,  $i=1$ , the special cases of double loss when two molecules react with each other and double generation of single molecules when size 2 particles dissociate are not counted exactly in Kampmann’s initial work. Thus the following revised balance equation is suggested here:

$$\frac{dn_1}{dt} = -n_1 \sum_{k=1}^{i_M} (1 + \delta_{1,k}) \beta_k n_k + \sum_{k=2}^{i_M} (1 + \delta_{2,k}) \alpha_k A_k n_k \quad [6]$$

Assuming a uniform spherical concentration field of single molecules with a boundary layer thickness of particle radius  $r_i$  around each size  $i$  particle, the diffusion growth rate of size  $i$  particle is expressed by<sup>[39]</sup>:

$$\beta_i = 4\pi D r_i \quad [7]$$

where  $D$  is the diffusion coefficient in the matrix phase. As precipitation reactions always involve more than one element, this coefficient is chosen for the slowest-diffusing element, which is assumed to control the diffusion rate.

The following relation is assumed for the dissociation rate, which is the number of molecules lost from the surface of size  $i$  particles per unit area per unit time, based on a mass balance of particles in equilibrium with the surrounding matrix phase<sup>[39]</sup>:

$$\alpha_i = \beta_i n_{1i} / A_i \quad [8]$$

The concentration of single molecules,  $n_{1i}$ , in equilibrium around the surface of each particle is needed to evaluate this equation. This is estimated using the Gibbs-Thompson equation, and decreases with increasing particle size as follows<sup>[51]</sup>:

$$n_{1i} = n_{1,eq} \exp\left(\frac{2\sigma V_P}{R_g T} \frac{1}{r_i}\right) \quad [9]$$

where  $n_{1,eq}$  is the number density of dissolved single molecules in equilibrium with a plane interface of the precipitate phase,  $\sigma$  is the interfacial energy between the precipitate particles and the matrix phase,  $V_P$  is the molar volume of the precipitate,  $R_g$  is the gas constant,  $T$  is the temperature. and  $r_i$  is the radius of size  $i$  particles. This equation indicates that increasing particle radius causes the nearby solute concentration to decrease greatly, by several orders of magnitude.

Results from equations [5]-[9] are considered to be the exact solution for diffusion test problems.

### 3. Particle-size-grouping (PSG) method

From a theoretical point of view, these models based on molecules in the previous section are accurate and the integration of their set of governing equations is straight forward. However, the computational cost quickly becomes infeasible for realistic particle sizes. The PSG method is introduced here to overcome this difficulty. The fundamental concept of the PSG method is shown schematically in Fig. 1. In this method, the particles are divided into different size groups (size group number  $j$ ) with characteristic volumes  $V_j$  and characteristic radius  $r_j$ . The number density of particles of size group  $j$  is defined as

$$N_j = \sum_{V_{j,j+1} > V > V_{j-1,j}} n(V) \quad [10]$$

This summation covers all particles whose volume lies between two threshold values. The threshold volume that separates two neighboring size groups,  $V_{jj+1}$ , is assumed to be the geometric average of the characteristic volumes of these two groups, instead of the arithmetic average used in previous works<sup>[46,47]</sup>:

$$V_{j,j+1} = \sqrt{V_j V_{j+1}} \quad [11]$$

If a newly generated particle has its volume between  $V_{j-1,j}$  and  $V_{jj+1}$ , it is counted in size group  $j$ . The increase of number density of size group  $j$  is then adjusted according to the difference between the volume of the new particle and  $V_j$ , in order to conserve mass.

The particle volume ratio between two neighboring size groups is defined as

$$R_V = \frac{V_{j+1}}{V_j} \quad [12]$$

In general,  $R_V$  need not be a constant. However, for constant  $R_V$ , the above variables simplify as

$$V_j = R_V^{j-1} V_1, \quad V_{j,j+1} = R_V^{(j-1/2)} V_1 \quad [13]$$

where the volume of a single molecule,  $V_1$ , is computed using the molar volume of its precipitate crystal structure,  $V_P$ :

$$V_1 = \frac{V_P}{N_A} \quad [14]$$

where  $N_A$  is Avogadro number, and the small effects of temperature change and vacancies are neglected. Since this volume is calculated from a bulk property,  $V_P$ , the packing factor is not needed. The number of molecules contained in the given volume is

$$m_j = \frac{V_j}{V_1}, \quad m_{j,j+1} = \frac{V_{j,j+1}}{V_1} \quad [15]$$

In the PSG method, it is easy to introduce fractal theory to consider the effect of particle morphology. The effective radius of a particle can be expressed by

$$r_j = r_1 \left( \frac{V_j}{V_1} \right)^{1/D_f} \quad [16]$$

where  $D_f$  is the fractal dimension, which can vary from 1 (needle-shaped precipitates) to 3 (complete coalescence). Tozawa<sup>[52]</sup> proposed  $D_f=1.8$  for  $Al_2O_3$  clusters in liquid steel, and  $D_f=3$  is adopted in this work for simplicity.

After the number of single molecules composing the largest agglomerated particles  $i_M$  is determined, the corresponding number of size groups  $G_M$  chosen for the PSG method to cover the complete size range must satisfy  $R_V^{G_M-1} > i_M$ . Thus  $G_M$  must satisfy:

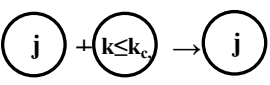
$$G_M \geq \text{ceil}(\log_{R_V} i_M) + 1 + 1 \quad [17]$$

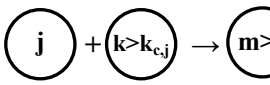
The largest size group is a boundary group which always has zero number density. The accuracy of the PSG method is expected to increase with smaller value of  $R_V$  since more size groups are used. From the logarithm relation shown above, the PSG method is far more efficient for real problems with a large range of particle sizes.

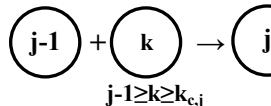
### 3.1 PSG method for collision

The following assumptions are made: a collision of size group  $j$  particle with smaller particle ranging from size group 1 to  $k_{c,j}$  still generates size group  $j$  particle with size larger than  $V_j$ , and a collision of size group  $j$  particle with particle larger than size group  $k_{c,j}$  generates particle in  $j+1$  or higher size group. Moreover, a collision of size group  $j-1$  particle with the particle ranging from size group  $k_{c,j}$  to  $j-1$  generates size group  $j$  particle. The corresponding coefficients are inserted before each term so as to conserve the volume. Consider all these assumptions to get the equation

$$\frac{dN_j}{dt} = \underbrace{N_j \sum_{k=1}^{k_{c,j}} \frac{V_k}{V_j} \Phi_{j,k} N_k}_{\text{Diagram 1}} - \underbrace{N_j \sum_{k=k_{c,j}+1}^{G_M} [(1+\delta_{j,k}) \Phi_{j,k} N_k]}_{\text{Diagram 2}} + \underbrace{\sum_{k=k_{c,j}}^{j-1} \frac{V_{j-1} + V_k}{V_j} \Phi_{j-1,k} N_{j-1} N_k}_{\text{Diagram 3}} \quad (j \geq 2) \quad [18]$$







with  $k_{c,j} = \begin{cases} j-1 & 4.000 > R_V > 2.148 \\ j-2 & 2.148 > R_V > 1.755 \\ j-3 & 1.755 > R_V > 1.587 \end{cases}$

The above values are given by solving the equations

$$V_j + V_{k_{c,j}+1} > V_{j,j+1} \quad [19]$$



The variables in equation [19] are defined as functions of  $R_V$  in Eq. [13], and this equation is solved to get values of  $R_V$  for different  $k_{c,j}$  as listed above.

The number density of single molecules to model collisions with the PSG method is calculated by

$$\frac{dN_1}{dt} = -N_1 \sum_{k=1}^{G_M} (1 + \delta_{1,k}) \Phi_{1,k} N_k \quad [20]$$

### 3.2 PSG method for diffusion

When the PSG method is applied to diffusion processes, adding a molecule to a particle does not always give enough particle growth to count it in the next larger size group. Thus, diffusion growth and dissociation must be carefully considered both inside and between size groups. Since particles governed by diffusion only gain or lose one individual molecule and the size groups  $j-1, j$  and  $j+1$  all influence the evolution of size group  $j$  number density during a given time interval, some knowledge of the particle distribution inside each size group is necessary. All particles inside a size group  $j$  will still stay in this group even after a diffusion growth or dissociation event, except for those bordering the neighboring size groups,  $n_j^L$  (closest to  $V_{j-1,j}$ ) and  $n_j^R$  (closest to  $V_{j,j+1}$ ). Size group  $j$  particles can be generated if particles  $n_{j-1}^R$  from size group  $j-1$  jump into size group  $j$  by diffusion growth or particles  $n_{j+1}^L$  from size group  $j+1$  fall into size group  $j$  by dissociation. At the same time, size group  $j$  particles can be lost if particles  $n_j^R$  jump to size group  $j+1$  by diffusion growth or particles  $n_j^L$  fall to size group  $j-1$  by dissociation. These considerations are incorporated into the new PSG method, taking care to conserve mass, as follows:

$$\begin{aligned} \frac{dN_j}{dt} = & \frac{m_1}{m_j} \beta_j N_1 (N_j - n_j^R) - \frac{m_1}{m_j} \alpha_j A_j (N_j - n_j^L) \\ & + \frac{\text{ceil}(m_{j-1,j})}{m_j} \beta_{j-1}^R N_1 n_{j-1}^R + \frac{\text{floor}(m_{j,j+1})}{m_j} \alpha_{j+1}^L A_{j+1}^L n_{j+1}^L \\ & - \frac{\text{floor}(m_{j,j+1})}{m_j} \beta_j^R N_1 n_j^R - \frac{\text{ceil}(m_{j-1,j})}{m_j} \alpha_j^L A_j^L n_j^L \quad (j \geq 2) \end{aligned}$$

with  $r_j^L = \left( \text{ceil}(m_{j-1,j}) \right)^{1/D_f} r_1$ ,  $r_j^R = \left( \text{floor}(m_{j,j+1}) \right)^{1/D_f} r_1$

$$\beta_j^L = 4\pi D_1 r_j^L, \quad \beta_j^R = 4\pi D_1 r_j^R$$

$$\alpha_j^L = \frac{\beta_j^L N_{1,eq}}{A_j^L} \exp\left(\frac{2\sigma V_P}{R_g T} \frac{1}{r_j^L}\right), \quad \alpha_j^R = \frac{\beta_j^R N_{1,eq}}{A_j^R} \exp\left(\frac{2\sigma V_P}{R_g T} \frac{1}{r_j^R}\right) \quad [21]$$

where  $n_j^L$  is the number density of those particles in size group  $j$  which fall into size group  $j-1$  by losing one molecule, and  $n_j^R$  is the number density of those particles in size group  $j$  which jump into size group  $j+1$  by gaining one molecule. Function *ceil* calculates the smallest integer which is not less than the given real number, and *floor* for the largest integer which is not larger than the given real number. The corresponding radius, diffusion growth rate and dissociation rate are also calculated for these particles. Since the mean and boundary (ceil, floor) values of size groups are utilized directly and  $R_V$  is not explicitly shown in equation, this formulation is very flexible to apply. This allows arbitrary size increment between groups, making it easy to improve accuracy with smaller  $R_V$  and improve computation with larger  $R_V$  in single simulation. The finer size groups need to be applied for the main size range of interest, and the group sizes could be chosen to fit the experiments.

In the above equation, the first and second terms on the right-hand side account for the diffusion growth and dissociation inside size group  $j$ , and third and fourth terms for generation of size group  $j$  particles by the inter-group diffusion growth and dissociation. The last two terms are for loss of size group  $j$  particles due to the diffusion growth and dissociation of size group  $j$  particles themselves.

For the diffusion population of single molecules in PSG method is given by

$$\begin{aligned} \frac{dN_1}{dt} = & -N_1 \sum_{k=1}^{G_M} (1 + \delta_{1,k}) \beta_k (N_k - n_k^R) + \sum_{k=2}^{G_M} \alpha_k A_k (N_k - n_k^L) \\ & - N_1 \sum_{k=1}^{G_M} (1 + \delta_{1,k}) \beta_k^R n_k^R + \sum_{k=2}^{G_M} (1 + \delta_{2,k}) \alpha_k^L A_k^L n_k^L \end{aligned} \quad [22]$$

The particle number densities  $n_j^L$  and  $n_j^R$  are estimated from geometric progression approximation

$$n_j^L = n_{j-1}^C \left( \frac{n_j^C}{n_{j-1}^C} \right)^{\frac{\text{ceil}(m_{j-1,j}) - m_{j-1}}{m_j - m_{j-1}}}, \quad n_j^R = n_j^C \left( \frac{n_{j+1}^C}{n_j^C} \right)^{\frac{\text{floor}(m_{j,j+1}) - m_j}{m_{j+1} - m_j}} \quad [23]$$

In order to propagate particle growth, if  $n_j^L \neq 0$  and  $n_{j+1}^C = 0$ ,  $n_j^R$  is calculated by

$$n_j^R = n_j^L \left( \frac{n_j^C}{n_j^L} \right)^{\frac{\text{floor}(m_{j,j+1}) - m_j}{m_{j+1} - m_j}} \quad [24]$$

The particle number density at center of each size group is calculated by assuming two geometric progressions inside the size group  $j$  such that

$$n_j^C = \frac{N_j}{\sum_{k=1}^{m_j - \text{ceil}(m_{j-1,j})} (1/q_j^L)^k + 1 + \sum_{k=1}^{\text{floor}(m_{j,j+1}) - m_j} (q_j^R)^k}$$

with 
$$q_j^L = \left( \frac{\bar{n}_j}{\bar{n}_{j-1}} \right)^{\frac{1}{m_j - m_{j-1}}}, \quad q_j^R = \left( \frac{\bar{n}_{j+1}}{\bar{n}_j} \right)^{\frac{1}{m_{j+1} - m_j}} \quad [25]$$

The average number density of size group  $j$  is calculated as

$$\bar{n}_j = \frac{N_j}{\text{floor}(m_{j,j+1}) - \text{ceil}(m_{j-1,j}) + 1} \quad [26]$$

#### 4. Validation of new PSG method with test problems

##### 4.1 Collision problem

Saffman<sup>[25]</sup> suggested a turbulent collision frequency in unit volume of liquid medium:

$$\Phi_{ij} = 1.3a(\mathcal{E}/\nu)^{1/2}(r_i + r_j)^3 \quad [27]$$

where  $\mathcal{E}$  is turbulent energy dissipation rate and  $\nu$  is kinematic viscosity. The empirical coefficient  $a$  was suggested by Higashitani<sup>[53]</sup> and it is assumed as a constant here. This model has been often applied to study the inclusion agglomeration in the liquid steel and chosen as our test problem for collision.

Choose the dimensionless forms for variables as

$$n_i^* = n_i / n_0, \quad t^* = 1.3a(\mathcal{E}/\nu)^{1/2} r_1^3 n_0 t \quad [28]$$

Here  $n_0$  and  $r_1$  are the initial number density and the radius of single molecules. The initial condition is given by  $n_i^* = 1$  for  $i=1$  and  $n_i^* = 0$  for  $i > 1$ . The size of largest agglomerated particle is  $i_M = 12000$ , such that 0.05% accuracy in the total volume of particles is guaranteed up to  $t^* = 1$ . The boundary condition is constantly zero number density for the largest agglomerated particle in exact solution or for the largest size group in PSG method. Runge-Kutta-Gill method is applied for integration and the time step is selected as  $\Delta t^* = 0.0025$  for accuracy, which is tested by comparing the results from smaller step size and negligible difference is found.

Total dimensionless number density of molecules and particles are defined as

$$N_M^* = \sum_{i=1}^{i_M} i \cdot n_i^*, \quad N_T^* = \sum_{i=1}^{i_M} n_i^* \quad \text{for exact solution}$$

$$N_M^* = \sum_{j=1}^{G_M} V_j \cdot N_j^*, \quad N_T^* = \sum_{j=1}^{G_M} N_j^* \quad \text{for PSG method} \quad [29]$$

The mass balance requires  $N_M^*$  to be constant in the whole calculation. In Fig. 2, we could see the total volume of particles is conserved for both exact solution and PSG method. There is also good agreement for total number density of particles for both cases of  $R_V = 3$  and  $R_V = 2$ . Fig. 3 shows that the change of the number densities of each size group with time and the PSG method also agrees well

with the exact solution for different  $R_V$ . For size group  $N_{10}$  in  $R_V=2$ , it contains all of the particle sizes ranging from 363 to 724 molecules, with a central size of 512 molecules. When time increases, collision always promotes large particles to form and small particles to disappear. With smaller value of  $R_V$ , the accuracy of PSG method increases as expected.

## 4.2 Diffusion problem

It is assumed the total number density of single molecules in system are produced by an isothermal first order reaction<sup>[39]</sup>

$$n_s^*(t^*) = n_s(t^*) / n_{1,eq} = \sum_{i=1}^{i_M} i \cdot n_i^* = 9[1 - \exp(-0.1t^*)] \quad [30]$$

Since  $n_s^*$  increases with time, the number density of dissolved single molecules must be adjusted with the increase of  $n_s^*$  at each time step. It could be also explained as the supersaturation increase when temperature drops in the practical cooling process.

The dimensionless forms are defined as

$$n_i^* = n_i / n_{1,eq}, \quad t^* = 4\pi D_1 r_1 n_{1,eq} t \quad [31]$$

Choose  $B=2\sigma V_P/(R_g Tr_1)=3.488$  for calculating dissociation rate. The initial condition is  $n_i^*=0$  for  $i \geq 1$ . The boundary condition is also zero number density for the largest agglomerated particle in exact solution or for the largest size group in PSG method all the time. The maximum size of agglomerated particle is chosen as  $i_M=50000$ , such that mass conservation is guaranteed up to  $t^*=10000$ . Runge-Kutta-Gill method was also used for integration and the time step is selected as  $\Delta t^*=0.01$  for accuracy.

As shown in Fig. 4, the total volume of particles is conserved for both exact solution and PSG method. Fig. 5 shows how the particle size distribution evolves due to the changing concentration gradients near particles of different size groups. At early times, all size group particles grow owing to the driving force of increasing supersaturation. At later times, the results show Ostwald ripening. The large particles have low concentrations, so tend to grow at the expense of smaller particles, which have high local concentrations, and eventually shrink. For example, size group  $N_1$  (dissolved single molecules) reaches its peak and starts to decrease in number after  $t^*=20$ . There are reasonable agreements for total particle number density and number densities of each size group between the PSG method and exact solution for both cases of  $R_V=3$  and  $R_V=2$ . The PSG method for  $R_V=2$  matches exact solution more closely.

The computation times of the above test problems are listed in Table I. All the calculations are run with Matlab on Dell OPTIPLEX GX270 with P4 3.20GHz CPU and 2GB RAM in order for comparison. The computational cost is found to dramatically reduce in PSG method. It is worth to mention that the computation cost for collision problem is proportional to  $i_M^2$  for exact solution or  $G_M^2$  for the PSG method, while proportional to  $i_M$  or  $G_M$  correspondingly for diffusion problem. Since the

details of particle distribution in size groups is calculated in diffusion problem, the time saving is not so significant. But this is enough to make practical precipitation calculations possible, considering that less than 60 size groups covers particle sizes up to 100 $\mu\text{m}$  with constant  $R_V=2$  for most nitrides and carbides.

## 5. Practical applications

When the PSG method [21] is applied to model a real precipitation process, it becomes essential to avoid stability problems due to dissociation exceeding diffusion growth. A stable scheme is required to apply a large time step size in simulation to enable reasonable computation times. Thus the implicit Euler scheme is adopted to integrate the equations through time:

$$\begin{aligned} & \left[ 1 + \Delta t \left( \frac{m_1}{m_j} \alpha_j A_j + \frac{\text{floor}(m_{j,j+1})}{m_j} \beta_j^R N_1^{i+1} + \frac{\text{ceil}(m_{j-1,j})}{m_j} \alpha_j^L A_j^L \right) \right] N_j^{i+1} \\ &= N_j^i + \Delta t \left[ \frac{m_1}{m_j} \beta_j N_1^{i+1} (N_j^{i+1} - n_j^R) + \frac{m_1}{m_j} \alpha_j A_j n_j^L + \frac{\text{ceil}(m_{j-1,j})}{m_j} \beta_{j-1}^R N_1^{i+1} n_{j-1}^R + \frac{\text{floor}(m_{j,j+1})}{m_j} \alpha_{j+1}^L A_{j+1}^L n_{j+1}^L \right. \\ & \quad \left. + \frac{\text{floor}(m_{j,j+1})}{m_j} \beta_j^R N_1^{i+1} (N_j^{i+1} - n_j^R) + \frac{\text{ceil}(m_{j-1,j})}{m_j} \alpha_j^L A_j^L (N_j^{i+1} - n_j^L) \right] \quad (j \geq 2) \end{aligned} \quad [32]$$

where  $i$  is the index of time step. The above system of equation is computed by iterative Gauss-Seidel method until the largest change of  $N_j^{i+1}$  converges to be less than  $10^{-5}$  between two iterations. The upper limits of  $n_j^L$  and  $n_j^R$  are  $N_j^{i+1}$ , and the values of  $n_j^L$  and  $n_j^R$  are evaluated at each iteration. Since the mass conservation is validated in test problems, the number density of single molecule is then computed as follows, in order to save computation:

$$N_1^{i+1} = n_s - \sum_{j=2}^{G_M} m_j N_j^{i+1} \quad [33]$$

where  $n_s$  is the total number density of molecules, which is determined by the steel composition. If the steel composition of element  $M$  is  $M_0$ , then the total number density of molecules in steel is calculated as

$$n_s = \frac{M_0 \rho_{\text{steel}}}{100 A_M} N_A \quad [34]$$

The equilibrium number density of single molecules in steel is calculated from its equilibrium dissolved mass concentration  $[M]$ , which is obtained from the equilibrium precipitation calculation

$$n_{1,eq} = \frac{[M] \rho_{\text{steel}}}{100 A_M} N_A \quad [35]$$

Where  $A_M$  is the atomic mass of element M, and  $\rho_{\text{steel}}$  is the density of steel matrix ( $7500\text{kg}\cdot\text{m}^{-3}$ ). Although the suggested scheme is stable for any time step size, the accuracy is maybe exacerbated if the time step is too large. Thus the reasonable time step is chosen when small difference is found if the time step continues to decrease.

### 5.1 Size distribution for isothermal NbC precipitation

In order to validate the ability of PSG model to simulate the size distribution of precipitate particle, the experimental results from Jones and Howell<sup>[54]</sup> is extracted for comparison. The steel has a composition of 20%Cr, 25%Ni, 0.5%Nb, 0.05%C+N. The case of the specimen solution treated at 1350°C, quenched and aged at 930°C for 1800s with no deformation prior to ageing is chosen to compare with simulation. The carbon extraction replicas were used in the acquisition of quantitative particle size distribution data. This technique is proved to be powerful to detect nuclei with the diameter of less than 2nm<sup>[55]</sup>. The truncating radius is set as 0.31nm to match experiments.

Since the individual compositions of carbon and nitrogen are not clear, the total 0.05% composition is assumed to be purely carbon in calculation because the alloying carbon in steel is always much plentiful than nitrogen. Since it is sufficient to react with Nb, the number density of NbC particles is calculated based on available carbon. Diffusion coefficient of Nb in austenite is taken as  $D_{\text{Nb}}(\text{m}^2/\text{s})=0.83\times 10^{-4}\exp(-266500/RT)$ <sup>[56]</sup>, molar volume of NbC is  $V_p=13.39\times 10^{-6}\text{m}^3/\text{mol}$ <sup>[57]</sup>. The value of interfacial energy is calculated in the appendix. The equilibrium calculation in Fig. 6 shows that the NbC precipitate begins to form at 1310°C, and the equilibrium dissolved mass concentration of carbon in steel is 0.0052426wt% at T=930°C. In order to compare with experimental data,  $R_f$  is not set as constant.  $R_f=2$  for particles with radius smaller than 3nm, 1nm size groups are used for 3-15nm, 1.5nm size groups for 15-24nm, 3nm size groups for 24-36nm, 6nm size groups for 36-48nm. Total 38 size groups are used to cover the particle size up to 48nm. Last size group must be set to cover the largest observed particle formed in experiments. The time step is set as 0.001s with maximum of iteration 10000 for convergence.

The measured particle size distribution/volume number frequency plot averaged over all of the matrix regions is normalized and compared with simulation results in Fig. 7. The actual mean radius of NbC particles were 9.3nm in experiment and 8.13nm in simulation and particle size distribution also matches reasonably. It is also observed that the measured size distribution is wider than the simulation results. The reason is that there are always large densities of grain boundaries and dislocations in steels where easier nucleation and higher diffusion rate are possible to form larger precipitate particles. Moreover, the uncertainty of carbon and nitrogen in the given steel composition will change the precipitate type from NbC to Nb(C,N), thus influence the equilibrium dissolved concentration

(supersaturation) and the interfacial energy of precipitate particles. The formation of other precipitates also can not be excluded, especially the chromium carbide and nitride due to the high concentration of chromium. If these precipitates form earlier and become the nucleation sites of NbC, the precipitation of NbC will be accelerated.

## 5.2 Precipitated fraction of isothermal AlN precipitation

The isothermal precipitation behavior for AlN in a 0.09%C, 0.20%Si, 0.36%Mn, 0.051%Al and 0.0073%N steel is measured by Vodopivec<sup>[58]</sup>. Specimens were first solution treated at 1300°C for 2 hours before being quenching to the precipitation temperature. The AlN content in steel was determined by the Beeghly method<sup>[59]</sup>. Since it has been suggested that Beeghly technique is insensitive to detect the presence of fine precipitate particles which could pass through the filter<sup>[60,61]</sup>, the truncating precipitate radius is set as 1.93nm in the simulation to match the measurements. The initial experimental measurements all start from nonzero value, possible because the cooling stage from solution treated temperature to precipitation temperature or the quenching stage after the precipitation test is not quick enough. The final precipitated amounts of nitrogen in AlN at each holding temperature could not reach their theoretical values calculated by equilibrium model, even when the precipitated fraction become nearly constant under very long holding time. It is maybe caused by the fact that other types of nitrides exist in steels. Thus the measurements are normalized with zero fractions at beginning and maximum value  $(N_0 - [N])/N_0$  at the entire precipitation process.

Diffusion coefficient of Al in austenite is taken as  $D_{Al}(m^2/s) = 2.51 \times 10^{-4} \exp(-253400/RT)^{[62]}$ , molar volume of AlN is  $V_p = 12.54 \times 10^{-6} m^3/mol^{[57]}$ . The interfacial energies are calculated by the method in appendix. The number densities of precipitate particles are calculated by the nitrogen concentration since it is insufficient when reacting with aluminum to form AlN. The experiments found that precipitation was much quicker in ferrite phase because of lower solubility limit of AlN and quicker diffusion rate of aluminum, the precipitation of AlN at 700°C is also simulated with the diffusion coefficient of Al in ferrite  $D_{Al}(m^2/s) = 0.3 \times 10^{-2} \exp(-234500/RT)^{[57]}$ .

As shown in Fig. 6, the equilibrium model<sup>[17]</sup> calculated the formation temperature of AlN is 1236°C, and the equilibrium dissolved concentration of nitrogen in steel is around 0.00022wt% at  $T=840^\circ C$  ( $\Pi_C=33.2$ ) and 0.0000031wt% at  $T=700^\circ C$  ( $\Pi_C=2370$ ). A sharp decrease of equilibrium dissolved aluminum concentration could be seen during  $\gamma \rightarrow \alpha$  phase transformation (within temperature range 865°C to 715°C) because of the solubility limit of AlN is much lower in ferrite, which is already carefully considered in the equilibrium model. Constant  $R_f=2$  and total 32 size groups are used in the simulation, and this covers particle radius up to around 200nm. The time step is set as 0.001s with maximum of iteration 10000 for convergence.

The numerical results are shown and compared with experimental measurements in Fig. 8, and good matches are found for precipitated AlN fractions at both isothermal annealing temperatures. The calculation verifies the experimental observation of greatly accelerated precipitation in ferrite even at a lower temperature. The calculated size distribution evolution of AlN particles at each annealing temperature are depicted in Fig. 9. The results show that at 700°C, because of high supersaturation and large diffusion rate, the diffusion growth stage finished within 90s, and the coarsening governs the remaining precipitation process. The particle size distribution at 840°C shows that the coarsening happens after 3100s since the increase of particle size becomes much slower after that. These precipitate finish times correspond well with the transition points of precipitated fractions, which changes from the sharp growth stage to the quite flat coarsening stage.

In this work, we do not introduce any fitting parameters in simulation, and the calculated particle size distribution of NbC and precipitated amount of AlN corresponds well with experiments. The better match could be obtained by more careful choice of involving physical parameters, such as equilibrium dissolved concentration (supersaturation), diffusion rate or interfacial energy. It is also worth to mention that the calculated results are deteriorated by the fact that there is always more than one type of precipitate formed in steels. Since the different precipitates will possibly compete with each other to attract the same elements, such as different nitrides attracting nitrogen, it is often not accurate to use the steel composition to simulate growth of single precipitate unless the equilibrium model strictly excludes the formation of other precipitates. The precipitates could form at different times in steels, and the previously formed precipitates will be the nucleation sites for the new precipitates. Thus it makes new precipitates nucleate and grow more easily, and the final property of multi-precipitates is obviously different from that of two separate precipitates case. Such a multi-precipitate growth model is maybe necessary in reality and being developed. Furthermore, the influence of deformation on precipitation kinetics is also not considered in the current work, but it actually increases the nucleation and growth rate of precipitation and cause a much finer particle size distribution<sup>[54,63]</sup>. These effects on precipitation behaviors need to be discussed in our future work.

## **Conclusions:**

1. A new general PSG method for particle collision has been derived for an arbitrary choice of size ratio  $R_V$  and good agreement has been verified with exact solutions.
2. A new, highly-efficient PSG method for diffusion-controlled particle growth has been developed. Results match the exact solution of Kampmann within a reasonable tolerance. The method features geometrically-based threshold values at the borders of each size group in order to accurately include



intra-group diffusion, corresponding accurate diffusion between size groups, and an efficient implicit solution method to integrate the equations.

3. The new PSG method can simulate particle nucleation, growth, and coalescence due to collision and diffusion over a wide size range or particles with low computational cost, high accuracy. Accuracy of the method increases with decreasing  $R_V$  as more size groups are used to cover the given particle size range.

4. The computed size distributions of NbC and the precipitated fraction of AlN match reasonably with previous experimental measurements in microalloyed steel without using any fitting parameters. Precipitation in ferrite is found to be greatly accelerated due to the lower solubility limit and higher diffusion rate of these precipitates in this phase.

5. The new PSG method is available to simulate realistic nonequilibrium precipitation behavior during various steel processes, such as continuous casting, for arbitrary temperature histories. Future work will incorporate other important effects into this kinetic model, such as multi-precipitate growth and deformation-induced precipitation.

#### Appendix: Calculation of interfacial energy

According to Turnbull<sup>[64]</sup> and Jonas<sup>[65]</sup>, the interfacial energy consists of two parts: one chemical part ( $\sigma_c$ ) and one structural part ( $\sigma_{st}$ ), so that

$$\sigma = \sigma_c + \sigma_{st} \quad [\text{A1}]$$

The coherent interfacial energy is estimated from the difference between the energies of bonding broken in the separation process and of bonds made in forming the interface, with only the nearest neighbors are considered. It is given by Russell as<sup>[32]</sup>

$$\sigma_c = \frac{\Delta E_0 N_s Z_s}{N_A Z_l} (X^P - X^M)^2 \quad [\text{A2}]$$

where  $\Delta E_0$  is the heat of solution of precipitate in a dilute solution of matrix,  $N_s$  is the number of atom per unit area across the interface,  $Z_s$  is the number of bonds per atom across the interface,  $Z_l$  is the coordinate number of nearest neighbors within the crystal lattice.  $\Delta E_0$  is estimated to equal  $-\Delta H$ , where  $\Delta H$  is the heat of formation of precipitate.

Van Der Merwe<sup>[66]</sup> presented the calculation for the planar interface. When the two phases have the same structure and orientation, but different lattice spacing, the mismatch may be accommodated by a planar array of edge dislocations. Accompanied with the strain energy in both crystals, the  $\sigma_{st}$  is given as

$$\sigma_{st} = \frac{\mu c}{4\pi^2} \left\{ 1 + \beta - (1 + \beta^2)^{1/2} - \beta \ln \left[ 2\beta(1 + \beta^2)^{1/2} - 2\beta^2 \right] \right\}$$

with  $\frac{2}{c} = \frac{1}{a_M^e} + \frac{1}{a_P^e}$ ,  $\frac{2}{\mu} = \frac{1}{\mu_M} + \frac{1}{\mu_P}$

$$\beta = 2\pi\delta \frac{\lambda_+}{\mu}, \delta = \frac{2|a_M^e - a_P^e|}{a_M^e + a_P^e}, \frac{1}{\lambda_+} = \frac{1 - \nu_M}{\mu_M} + \frac{1 - \nu_P}{\mu_P} \quad [\text{A3}]$$

where  $a_M^e$  and  $a_P^e$  are the effective nearest-neighbor distance across the interface, which are estimated from the lattice parameters  $a_M$ ,  $a_P$  and interface orientations.  $\mu_M$ ,  $\mu_P$  and  $\mu$  are shear modulus,  $\nu_M$  and  $\nu_P$  are Poisson's ratio. The subscript M, P and no subscript stand for the properties of matrix phase, precipitate and interface.  $\delta$  is calculated as the lattice misfit across the interface.

The crystallographic relationships between the AlN (h.c.p.), NbC (f.c.c.) and austenite phase (f.c.c.) are chosen as

$$(111)_{NbC} // (111)_{\gamma-Fe}^{[32,65]} \text{ and } (0001)_{AlN} // (111)_{\gamma-Fe}^{[67,68]}$$

The physical properties in the calculation are

$$-\Delta H_{AlN} (KJ / mol) = 341.32 - 4.98 \times 10^{-2} T - 1.12 \times 10^{-6} T^2 - 2813 / T^{[69]}$$

$$-\Delta H_{NbC} (KJ / mol) = 157.76 - 4.54 \times 10^{-2} T - 3.84 \times 10^{-6} T^2^{[70]}$$

$$\mu_{\gamma-Fe} (Gpa) = 81[1 - 0.91(T - 300)/1810]^{[71]}, \nu_{\gamma-Fe} = 0.29^{[72]}, a_{\gamma-Fe} (nm) = 0.357^{[57]}$$

$$\mu_{AlN} (Gpa) = 127^{[73]}, \nu_{AlN} = 0.23^{[73]}, a_{AlN} (nm) = 0.311, c_{AlN} (nm) = 0.497^{[57]}$$

$$\mu_{NbC} (Gpa) = 134[1 - 0.18(T - 300)/3613]^{[71]}, \nu_{NbC} = 0.194^{[71]}, a_{NbC} (nm) = 0.446^{[57]}$$

For  $\gamma$ -Fe (111) plane,  $Z_l^{\gamma-Fe} = 12$ ,  $Z_s^{\gamma-Fe} = 3$  and  $N_s^{\gamma-Fe} = 4/(\sqrt{3}a_{\gamma-Fe}^2)$ . The calculated interfacial energy increases slightly as temperature decreases, and the values used in the isothermal ageing simulations are

$$\sigma_{AlN}^{\gamma-Fe} (840^\circ C) = 0.908 J / m^2, \sigma_{AlN}^{\alpha-Fe} (700^\circ C) = 0.997 J / m^2$$

$$\sigma_{NbC}^{\gamma-Fe} (930^\circ C) = 0.540 J / m^2$$

## References:

1. C. Zener (quoted by C.S. Smith), Grain, phases, and interfaces: an interpretation of microstructure. *Trans. Am. Inst. Miner. Metall. Soc.*, 1948, vol.175, pp. 15-51.
2. M. Hillert, On the theory of normal and abnormal grain growth, *Acta Metallurgica*, 1965, vol. 13, pp.227-238.
3. T. Gladman, On the theory of the effect of precipitate particles on grain growth in metals, *Proceedings of the Royal Society of London*, series A, 1966, vol. 294, pp. 298-309.

4. P. A. Manohar, M. Ferry and T. Chandra, Five decades of the Zener equation, *ISIJ International*, 1998, vol. 38, pp. 913-924.
5. N. Yoshinaga, K. Ushioda, S. Akamatsu and O. Akisue, Precipitation Behavior of Sulfides in Ti-added Ultra Low-carbon Steels in Austenite, *ISIJ International*, 1994, vol.34, pp. 24-32.
6. E. E. Kashif, K. Asakura, T. Koseki and K. Shibata, Effect of Boron, Niobium and Titanium on Grain Growth in Ultra High Purity 18% Cr Ferritic Stainless Steel, *ISIJ International*, 2004, vol.44, pp. 1568-1575.
7. S. C. Park, I. H. Jung, K. S. OH and H. G. LEE, Effect of Al on the Evolution of Non-metallic Inclusions in the Mn-Si-Ti-Mg Deoxidized Steel During Solidification: Experiments and Thermodynamic Calculations, *ISIJ international*, 2004, vol.44, pp. 1016-1023.
8. Y. Li, J. A. Wilson, D. N. Crowther, P. S. Mitchell, A. J. Craven and T. N. Baker, The Effect of Vanadium, Niobium, Titanium and Zirconium on the Microstructure and Mechanical Properties of Thin Slab Cast Steels, *ISIJ International*, 2004, vol.44, pp. 1093-1102.
9. R. L. Klueh, K. Shiba and M. A. Sokolov, Embrittlement of irradiated ferritic/martensitic steels in the absence of irradiating hardening, *Journal of Nuclear Materials*, 2008, vol. 377, pp. 427-437.
10. J. Y. Choi, B. S. Seong, S. C. Baik and H. C. Lee, Precipitation and Recrystallization Behavior in Extra Low Carbon Steels, *ISIJ International*, 2002, vol.42, pp. 889-893.
11. B. J. Lee, Thermodynamic Assessment of the Fe-Nb-Ti-C-N system, *Metallurgical and Materials Transactions A*, 2001, vol.32, pp. 2423-2439.
12. R. C. Hudd, A. Jones and M. N. Kale, A method for calculating the solubility and composition of carbonitride precipitates in steel with particular reference to niobium carbonitride, *The Journal of the Iron and Steel Institute*, 1971, vol.209, pp. 121-125.
13. T. Gladman, *The Physical Metallurgy of Microalloyed Steels*, The Institute of Materials, London, England, 1997, chapter 3, Solubility of Microalloy Carbides and Nitrides, pp. 82-130.
14. W. J. Liu and J. J. Jonas, Calculation of the  $\text{Ti}(\text{C}_y\text{N}_{1-y})\text{-Ti}_4\text{C}_2\text{S}_2\text{-MnS}$ -Austenite equilibrium in Ti-bearing steels, *Metallurgical Transactions A*, 1989, vol.20A, pp. 1361-1374.
15. N. Gao and T. N. Baker, Influence of AlN Precipitation on Thermodynamic Parameters in C-Al-V-N Microalloyed Steels, *ISIJ International*, 1997, vol. 37, pp. 596-604.
16. J. Y. Park, J. K. Park and W. Y. Choo, Effect of Ti Addition on the Potency of MnS for Ferrite Nucleation in C-Mn-V Steels, *ISIJ International*, 2000, vol. 40, pp. 1253-1259.
17. K. Xu, B. G. Thomas, R. O'Malley, Equilibrium model of precipitation in microalloyed steels, Accepted by *Metallurgical and Materials Transactions A*, 2010.
18. A. N. Kolmogorov, On the static theory of crystallization of metals, *Izv. Akad. Nauk SSSR, Ser. Fiz.*, 1937, vol. 1, 335 [Bull. Acad. Sci. USSR, Phys. Ser., 1937, vol.1, 335].
19. W. A. Johnson and R. F. Mehl, Reaction kinetics in progresses of nucleation and growth, *Trans. AIME*, 1939, vol. 135, pp. 416-442.

20. M. Avrami, *J. Chem. Phys.*, Kinetics of phase change I. general theory 1939, vol.7, 1103; Kinetic of phase change II. Transformation-time relation for random distribution for nuclei, 1940, vol.8, 212; Kinetics of phase change III. Granulation, phase change and microstructure, 1941, 9, 177.
21. J. W. Christian, *The Theory of Transformation in Metals and Alloys*, Part I, Pergamon Press, Oxford, 1975, Chapter 12.
22. N. Y. Zolotarevsky, V. P. Pletenev and Y. F. Titovets, Analysis of aluminum nitride precipitation proceeding concurrently with recrystallization in low-carbon steel, *Modelling and Simulation in Materials Science and Engineering*, 1998, vol. 6, pp. 383-291.
23. H. C. Kang, S. H. Lee, D. H. Shin, K. J. Lee, S. J. Kim and K. S. Lee, Quantitative analysis of precipitation behavior in ferrite of V added microalloyed steel, *Materials Science Forum*, 2004, vol. 449-452, pp. 49-52.
24. M. Smoluchowski, Versuch einer mathematischen theorie der koagulationskinetic kolloider losungen, *Z. Phys. Chem.*, 1917, 92, pp. 127~155.
25. P. G. Saffman and J. S. Turner, On the Collision of Drops in Turbulent Clouds, *Journal of Fluid Mechanics*, 1956, 1, pp. 16-30.
26. U. Lindborg and K. Torssell, A collision model for the growth and separation of deoxidation products, *Transactions of Metallurgical Society of AIME*, 1968, 242, pp. 94-102.
27. S. K. Friedlander and C. S. Wang, The self-preserving particle size distribution for coagulation by Brownian motion, *Journal of Colloid and Interface Science*, 1966, vol. 22, pp. 126-132.
28. V. G. Levich, *Physicochemical hydrodynamics*, Prentice-Hall, Inc., Englewood Cliffs, NJ, 1962, pp. 211.
29. D. Turnbull and J. C. Fisher, Rate of nucleation in condensed systems, *The Journal of Chemical Physics*, 1949, vol. 17, pp. 71-73.
30. W. J. Liu and J. J. Jonas, Nucleation kinetics of Ti carbonitride in microalloyed austenite, *Metallurgical Transaction A*, 1989, vol.20A, pp. 689-697.
31. W. J. Liu and J. J. Jonas, A stress relaxation method for following carbonitride precipitation in austenite at hot working temperatures, *Metallurgical Transactions A*, 1988, vol.19A, pp. 1403-1413.
32. W. Ostwald, *Lehrbruck der allgemeinen Chemie*, 1896, vol.2, Leipzig, Germany.
33. I. M. Lifshitz and V. V. Slyozov, The kinetics of precipitation from supersaturated solid solutions, *Journal of Physics and Chemistry of Solids*, 1961, 19, pp. 35-50.
34. C. Wagner, Theorie der alterung von niederschlägen durch umloesen (Ostwald-Reifung), *Zeitschrift Elektrochemie*, 1961, 65, pp. 581-591
35. C. Zener, Theory of growth of spherical precipitates from solid solution, *Journal of Applied Physics*, 1949, vol. 20, pp. 950-953.
36. K. C. Russell, Nucleation in solid: the induction and steady state effects, *Advances in Colloid and Interface Science*, 1980, vol. 13, pp. 205-318.

37. H. I. Aaronson, L. Laird and K. R. Kinsman, Mechanisms of diffusional growth of precipitate crystals, *Phase Transformations*, edited by H. I. Aaronson, 1970, Metal Park, OH, ASM, pp. 313-396.
38. M. Kahlweit, Ostwald ripening of precipitates, *Advances in Colloid and Interface Science*, 1975, vol. 5, pp. 1-35.
39. L. Kampmann, M. Kahlweit, On the Theory of Precipitation II, *Berichte der Bunsen-Gesellschaft Physikalische Chemie*, 1970, vol. 74, pp. 456-462.
40. Y. Miki, B. G. Thomas, A. Denissov and Y. Shimada, Model of inclusion removal during RH degassing of steel, *Iron and Steelmaker*, 1997, vol. 24, pp. 31-38.
41. Y. Miki and B. G. Thomas, Modeling of inclusion removal in a tundish, *Metallurgical and Materials Transactions B*, 1999, 30B, pp. 639-654.
42. L. Zhang, S. Taniguchi and K. Cai, Fluid flow and inclusion removal in continuous casting tundish, *Metallurgical and Materials Transactions B*, 2000, 31B, pp. 253-266.
43. D. Sheng, M. Söder, P. Jönsson and L. Jonsson, Modeling micro-inclusion growth and separation in gas-stirred ladles, *Scandinavian Journal of Metallurgy*, 2002, vol. 31, pp. 134-147.
44. M. Hallberg, P. G. Jönsson, T. L. I. Jonsson and R. Eriksson, Process model of inclusion separation on a stirred steel ladle, *Scandinavian Journal of Metallurgy*, 2005, vol. 34, pp. 41-56.
45. N. Zhang and Z. C. Zheng, A collision model for a large number of particles with significantly different sizes, *Journal of Physics D: Applied Physics*, 2007, 40, pp. 2603-2612.
46. T. Nakaoka, S. Taniguchi, K. Matsumoto and S. T. Johansen, Particle-Size-Grouping method of inclusion agglomeration and its application to water model experiments, *ISIJ international*, 2001, 41, pp. 1103-1111.
47. L. Zhang and W. Pluschkell, Nucleation and growth kinetics of inclusions during liquid steel deoxidation, *Ironmaking and Steelmaking*, 2003, vol.30, pp. 106-110.
48. J. Zhang and H. Lee, Numerical modeling of nucleation and growth of inclusions in molten steel bases on mean processing parameters, *IJJ international*, 2004, vol. 44, pp. 1629-1638.
49. F. Gelbard, Y. Tambour and J. H. Seinfeld, Sectional representations for simulating aerosol dynamics, *Journal of Colloid and Interface Science*, 1980, vol. 76, pp. 541-556.
50. J. J. Wu and R. C. Flagan, A discrete-sectional solution to the aerosol dynamic equation, *Journal of Colloid and interface Science*, 1988, vol. 123, pp. 339-352.
51. J. M. B. Krishnamachari, B. Cooper and J. Stehna, Gibbs-Thomas formula for small island sizes: corrections for high vapor densities, *Physical Review B*, 1996, vol. 54, pp. 8899-8907.
52. H. Tozawa, Y. Kato, K. Sorimachi and T. Nakanishi, Agglomeration and Flotation of Alumina Clusters in Molten Steel, *ISIJ international*, 1999, 39, 426-434.
53. K. Higashitani, Y. Yamauchi, Y. Matsuno and G. Hosokawa, *Journal of Chemical Engineering of Japan*, 1983, 116, 299-304.

54. A. R. Jones, P. R. Howell and B. Ralph, Quantitative aspects of precipitation at grain boundaries in an austenitic stainless steel, *Journal of Materials Science*, 1976, vol.11, pp. 1600-1606.
55. H. J. Jun, K. B. Kang and C. G. Park, Effects of cooling rate and isothermal holding on the precipitation behavior during continuous casting of Nb-Ti bearing HSLA steels, *Scripta Materialia*, 2003, vol. 49, 1081-1086.
56. J. Geise and C. Herzig, Lattice and grain boundary diffusion of niobium in iron, *Z. Metallkd*, 1985, vol. 76, pp. 622-626.
57. I. T. Gladman, *The Physical Metallurgy of Microalloyed Steels*, The Institute of Materials, London, England, 1997, pp. 206-207.
59. F. Vodopivec, Technical note: On the influence of hot deformation of low-carbon steel by rolling on the precipitation of aluminium nitride, *Journal of The Iron and Steel Institute*, 1973, pp. 664-665.
59. H. F. Beeghly, Determination of combined nitrogen in steel: a rapid method, *Industrial and Engineering Chemistry*, 1942, vol.14, pp. 137-140.
60. W. C. Leslie, R. L. Rickett, C. L. Dotson and C. S. Walton, Solution and precipitation of aluminum nitride in relation to the structure of low-carbon steel, *Transactions of the American Society for Metals*, 1954, vol. 46, pp. 1470-1499.
61. F. G. Wilson and T. Gladman, Aluminium nitride in steel, *International Materials Review*, 1988, vol. 33, pp. 221-286.
62. H. Oikawa, Lattice diffusion in iron-a review, *Tetsu-To-Hagane*, 1982, vol. 68, pp. 1489-1497 (in Japanese).
63. J. P. Michel and J. J. Jonas, Precipitation kinetics and solute strengthening in high temperature austenites containing Al and N, *Acta Metallurgica*, 1981, vol. 28, pp. 513-526.
64. D. Turnbull, Role of structural impurities in phase transformations, *Impurities and imperfections*, Seminar Proceedings, American Society for Metals, Cleveland, OH, 1955, pp. 121-144.
65. W. J. Liu and J. J. Jonas, Characterisation of critical nucleus/matrix interface: application to Cu-Co alloys and microalloyed austenite, *Materials Science and Technology*, 1989, vol.5, pp. 8-12.
66. J. H. Van Der Merwe, Crystal interfaces, part I. semi-infinite crystals, *Journal of Applied Physics*, 1963, vol. 34, pp. 117-122.
67. H. Shoji, Geometric relationship between the structures of the modifications of a substance, *Zeitschrift fuer Kristallographie, Kristallgeometrie, Kristallphysik, Kristallchemie*, 1931, vol. 77, pp. 381-410.
68. Z. Nishiyama, *Science Report*, Tohoku Imperial Univ., 1936, 1st Ser. **25**, pp. 79.
69. Chase, M.W., Jr., NIST-JANAF Thermochemical Tables, Fourth Edition, *J. Phys. Chem. Ref. Data*, Monograph 9, 1998, pp. 1-1951.
70. L. E. Toth, *Transaction Metal Carbides and Nitrides*, Academic Press, New York, 1971.

71. H.J. Frost and M.F. Ashby: *Deformation-Mechanism Maps*, Pergamon Press, Oxford, United Kingdom, 1982, pp. 20-70.
72. L. M. Cheng, E. B. Hawbolt and T. R. Meadowcroft, Modeling of dissolution, growth and coarsening of aluminum nitride in low-carbon steels, *Metallurgical and Materials Transactions A*, 2000, vol.31A, pp. 1907-1916.
73. L. R. Zhao, K. Chen, Q. Yang, J. R. Rodgers and S.H. Chiou, Materials informatics for the design of novel coating, *Surface and Coating Technology*, 2005, vol. 200, pp. 1595-1599.

#### **Nomenclatures:**

- $a$  : Empirical coefficient for turbulence collision
- $f$  : Transformed fraction in phase transformation
- $i_M$  : Number of molecules for the largest agglomerated particle in simulation
- $n$  : Avrami exponent in KJMA model
- $n_0$  : Initial total number density of single molecules for collision problem ( $\# \cdot \text{m}^{-3}$ )
- $n_{1,eq}$  : Equilibrium concentration of dissolved single molecules for diffusion problem ( $\# \cdot \text{m}^{-3}$ )
- $n_i$  : Number density of size  $i$  particles ( $\# \cdot \text{m}^{-3}$ )
- $n_s$  : Released number density of single molecules for diffusion problem ( $\# \cdot \text{m}^{-3}$ )
- $n_j^C$  : Number density of particles at the center of size group  $j$  ( $\# \cdot \text{m}^{-3}$ )
- $n_j^C$  : Number density of particles inside size group  $j$ , which fall into size group  $j-1$  after losing one single molecule ( $\# \cdot \text{m}^{-3}$ )
- $n_j^U$  : Number density of particles inside size group  $j$ , which jump into size group  $j+1$  after getting one single molecule ( $\# \cdot \text{m}^{-3}$ )
- $r_i(r_j)$  : Characteristic radius of size  $i$  particles (or size group  $j$  particles) (m)
- $r_{j-1,j}$  : Threshold radius to separate size group  $j-1$  and size group  $j$  particles in PSG method (m)
- $r_c$  : The critical radius for nucleation (m)
- $t$  : Time (s)
- $\Delta t$  : Time step size in numerical computation (s)
- $A_i(A_j)$  : The surface area of size  $i$  particles (or size group  $j$  particles) ( $\text{m}^2$ )
- $A_M$  : Atomic mass unit of element M ( $\text{g} \cdot \text{mol}^{-1}$ )
- $D$  : Diffusion coefficient of the precipitation in the parent phase ( $\text{m}^2 \cdot \text{s}^{-1}$ )

$D_f$ : Fractal dimension for precipitate morphology  
 $G_M$ : Number of size groups for the largest agglomerated particle in PSG method  
 $K$ : Rate function for nucleation and growth in KJMA model  
 $N_j$ : Total number density of size group  $j$  particles in PSG method ( $\# \cdot \text{m}^{-3}$ )  
 $N_A$ : Avogadro number ( $6.022 \times 10^{23} \# \cdot \text{mol}^{-1}$ )  
 $N_M$ : Total number density of molecules ( $\# \cdot \text{m}^{-3}$ )  
 $N_T$ : Total number density of particles ( $\# \cdot \text{m}^{-3}$ )  
 $R_g$ : Gas constant ( $8.314 \text{ J} \cdot \text{K}^{-1} \cdot \text{mol}^{-1}$ )  
 $R_V$ : Particle volume ratio between two neighboring particle size groups  
 $T$ : Absolute temperature (K)  
 $V_i(V_j)$ : Characteristic volume of size  $i$  particles (or size group  $j$  particles) ( $\text{m}^3$ )  
 $V_{j-1,j}$ : Threshold volume to separate size group  $j-1$  and size group  $j$  particles in PSG method ( $\text{m}^3$ )  
 $V_p$ : Molar volume of precipitated phase ( $\text{m}^3 \cdot \text{mol}^{-1}$ )  
 $Z$ : Zeldovich nonequilibrium factor  
 $Z_s$ : Number of bonds per atom across the interface  
 $Z_l$ : Coordinate number of nearest neighbors within the crystal lattice  
 $\alpha_i$ : Dissociation rate of size  $i$  particles ( $\#^{-1} \cdot \text{m}^{-2} \cdot \text{s}^{-1}$ )  
 $\beta_i$ : Diffusion growth rate of size  $i$  particles ( $\text{m}^3 \cdot \#^{-1} \cdot \text{s}^{-1}$ )  
 $\delta_{i,k}$ : Kronecker's delta function  
 $\mathcal{E}$ : Turbulent energy dissipation rate ( $\text{m}^2 \cdot \text{s}^{-3}$ )  
 $\nu$ : Kinematic viscosity ( $\text{m}^2 \cdot \text{s}^{-1}$ )  
 $\rho_{steel}$ : Density of steel ( $\text{kg} \cdot \text{m}^{-3}$ )  
 $\rho_p$ : Density of precipitates ( $\text{kg} \cdot \text{m}^{-3}$ )  
 $\sigma$ : Interfacial energy between precipitated particle and steel matrix ( $\text{J} \cdot \text{m}^{-2}$ )  
 $\Phi_{i,k}$ : Collision kernel between size  $i$  and size  $k$  particles ( $\text{m}^3 \cdot \#^{-1} \cdot \text{s}^{-1}$ )  
 $\Delta E_0$ : Heat of solution of precipitate in a dilute solution of matrix ( $\text{J} \cdot \text{mol}^{-1}$ )  
 $\Delta H$ : Heat of formation of precipitate ( $\text{J} \cdot \text{mol}^{-1}$ )



Superscripts:

\* : Dimensionless value

– : Average value

Functions:

$ceil(x)$  : The smallest integer which is no less than real number  $x$

$floor(x)$  : The largest integer which is no larger than real number  $x$

Table I. Comparison of computational cost for test problems

	Collision ( $t^*=1$ )			Diffusion ( $t^*=10000$ )		
	Exact	PSG( $R_v=2$ )	PSG( $R_v=3$ )	Exact	PSG( $R_v=2$ )	PSG( $R_v=3$ )
Storage	$n_M=12000$	$N_G=16$	$N_G=11$	$n_M=50000$	$N_G=18$	$N_G=13$
Computational time	$\sim 225$ hours	$\sim 0.8s$	$\sim 0.4s$	$\sim 27$ hours	$\sim 560s$	$\sim 390s$

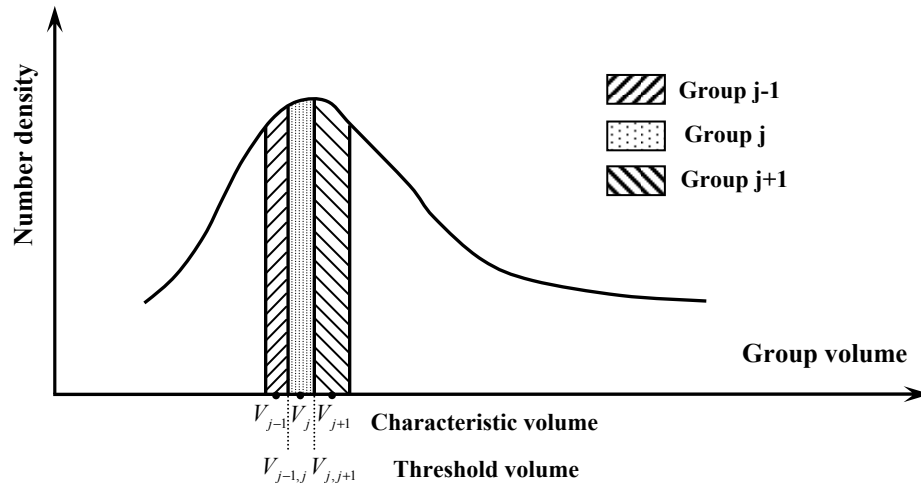


Fig.1–The schematic of particle size distribution in PSG method

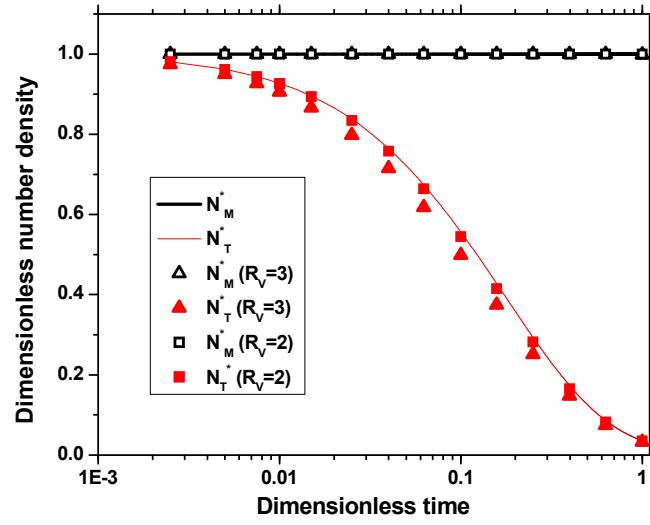
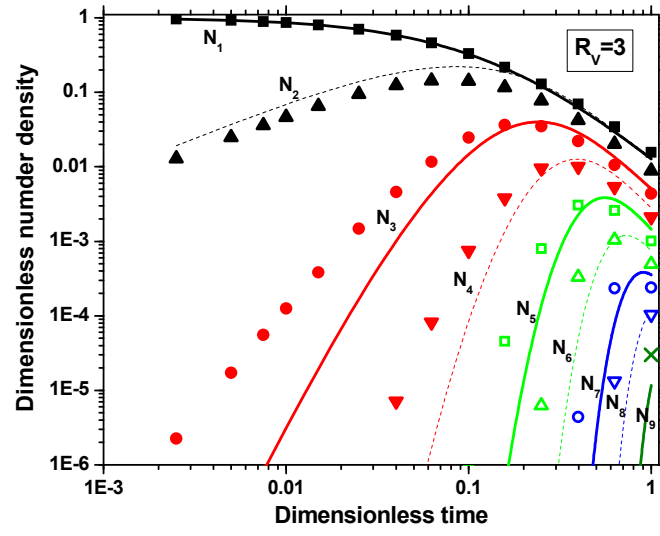
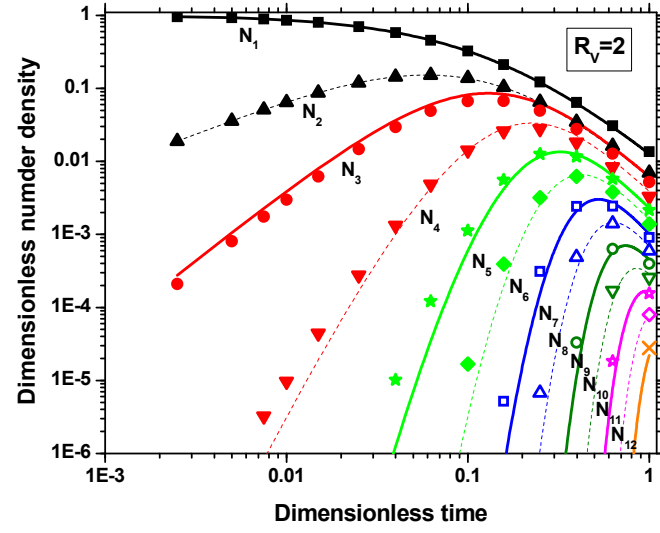


Fig.2—Comparison of collision curve calculated by PSG method with exact solution for different  $R_V$



(a).  $R_V=3$



(b).  $R_V=2$

Fig.3—Comparison of collision curve of each size group calculated by PSG method with exact solution for different  $R_V$

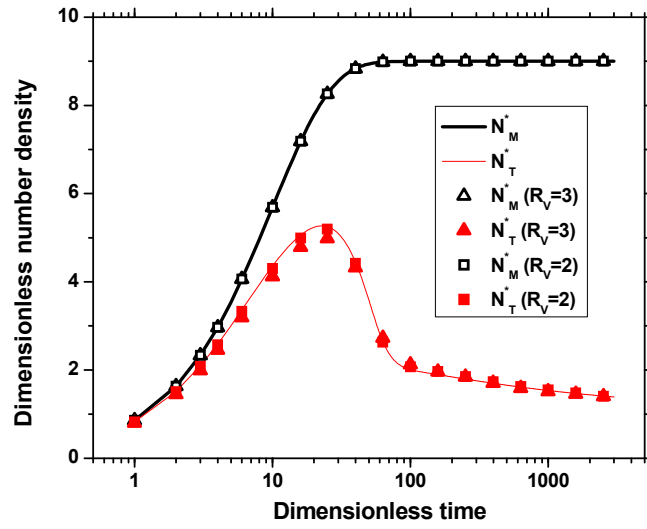
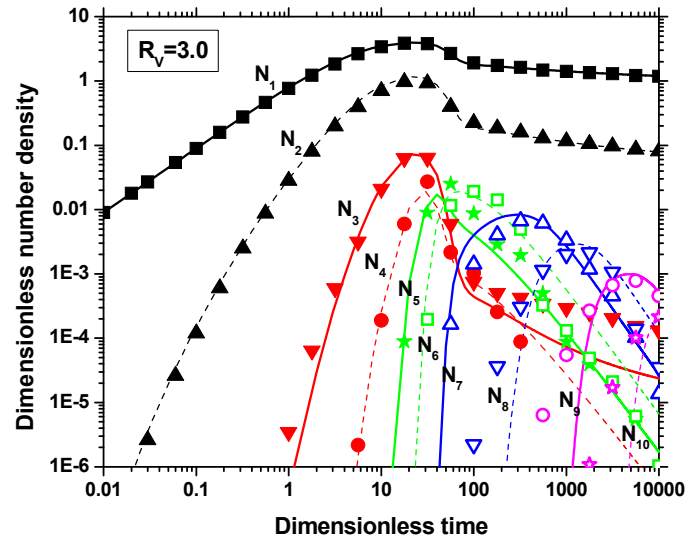
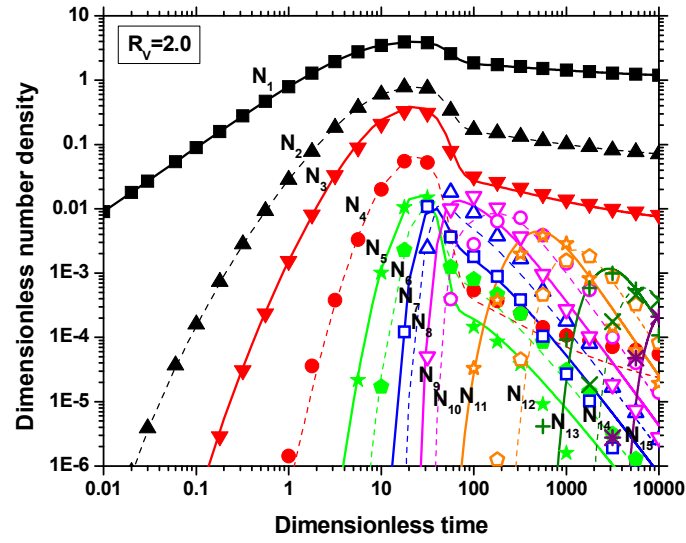


Fig.4—Comparison of diffusion curve calculated by PSG method with exact solution for different  $R_V$



(a).  $R_V=3$



(b).  $R_V=2$

Fig.5—Comparison of diffusion curve of each size group calculated by PSG method with exact solution for different  $R_V$

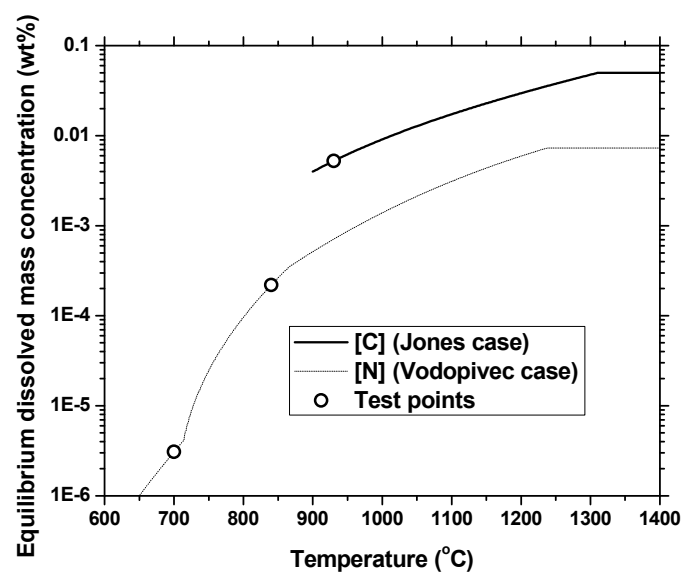


Fig.6—Calculated equilibrium dissolved mass concentration of C for Jones case<sup>[54]</sup> and N for Vodopivec case<sup>[58]</sup>

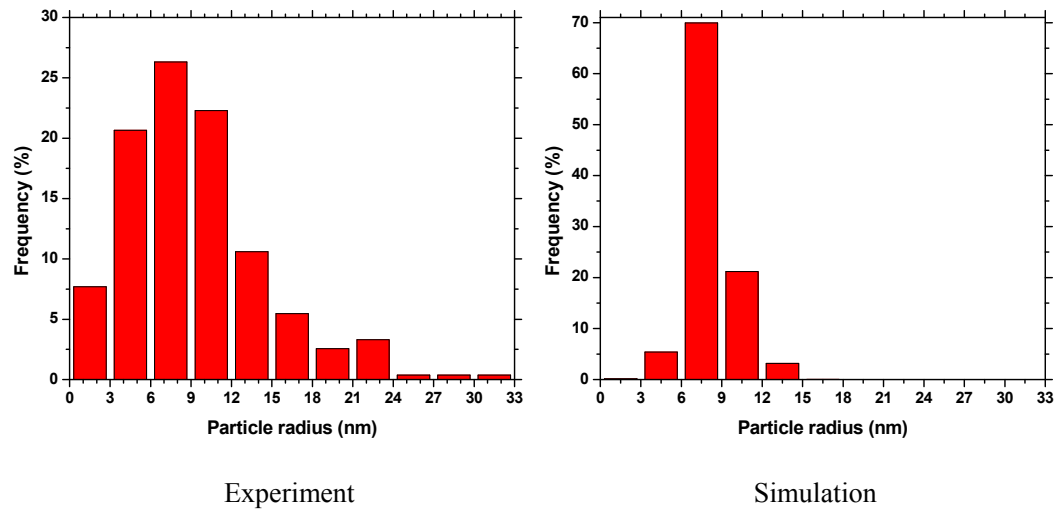


Fig.7–Calculated and measured frequency/size distribution plot of matrix particles obtained from specimens which were undeformed prior to ageing at 930°C for 1800s (experimental data from Jones<sup>[56]</sup>)

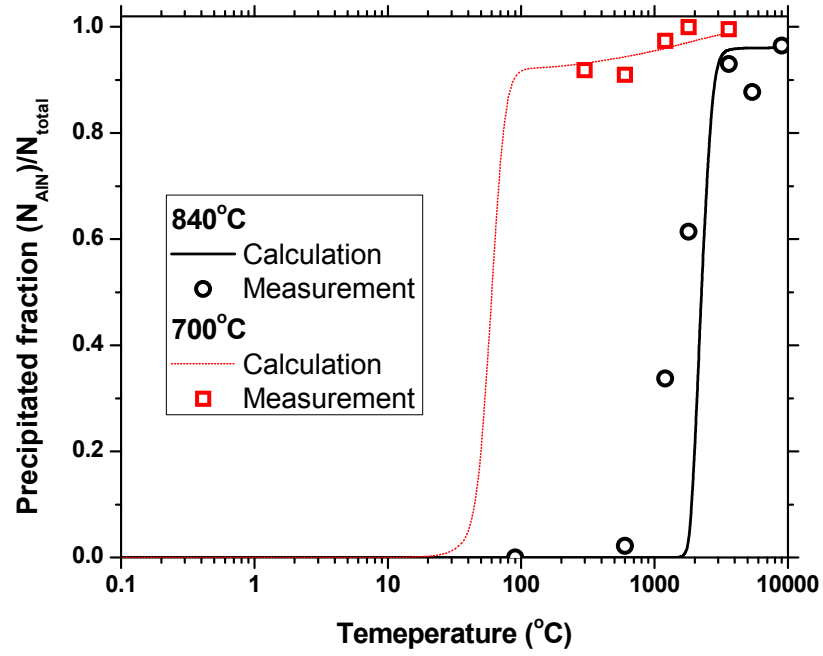
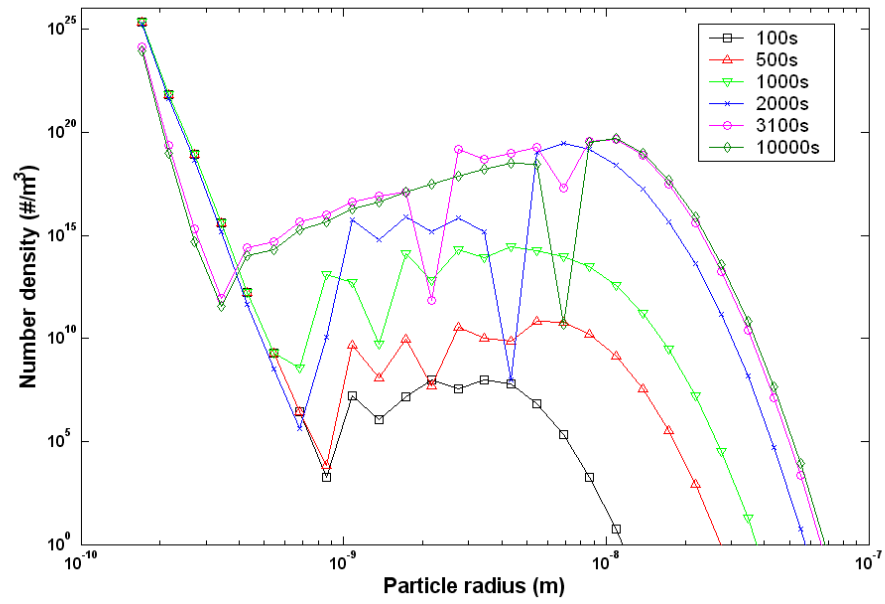
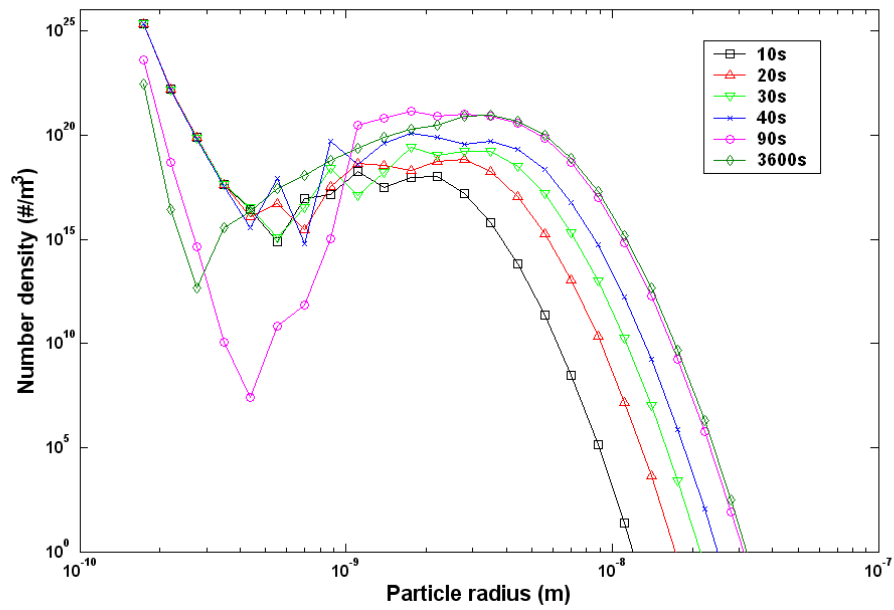


Fig.8—Calculated and measured precipitated fraction of AlN in a 0.051wt%Al and 0.0073wt%N steel during isothermal annealing at 840 $^{\circ}C$  and 700 $^{\circ}C$  (experimental data from Vodopivec<sup>[54]</sup>)





(a). 840°C



(b). 700°C

Fig.9—Calculated size distribution of AlN particles for a 0.051wt%Al and 0.0073wt%N steel at isothermal annealing temperature 840°C and 700°C